Estimate of soil hydraulic properties from disc infiltrometer three-dimensional infiltration curve. Numerical analysis and field application

B. Latorre [a*], C. Peña [a], L., Lassabatere[b], R. Angulo-Jaramillo [b], D. Moret-Fernández [a]

[a] Departamento de Suelo y Agua, Estación Experimental de Aula Dei, Consejo Superior de Investigaciones Científicas (CSIC), PO Box 13034, 50080 Zaragoza, Spain

[b] Université de Lyon; UMR5023 Laboratoire d'Ecologie des Hydrosystèmes Naturels et Anthropisés; Université Lyon 1; ENTPE; CNRS; 3, rue Maurice Audin, 69518 Vaulx-en-Velin, France

* Corresponding author. E-mail: borja.latorre@csic.es Tel.: (+34) 976 71 60 42

Abstract

Based on the analysis of Haverkamp et al. (1994), this paper presents a new technique to estimate the soil hydraulic properties (sorptivity, S, and hydraulic conductivity, K) from the full-time cumulative infiltration curves. The proposed method, which will be named as the Numerical Solution of the Haverkamp equation (NSH), was validated on 12 synthetic soils simulated with HYDRUS-3D. The K values used to simulate the synthetic curves were compared to those estimated with the NSH method. A procedure to detect and remove the effect of the contact sand layer on the cumulative infiltration curve was also developed. A sensitivity analysis was performed using the water level measurement as uncertainty source and the procedure was evaluated considering different infiltration times and data noise (e.g. air-bubbling in the infiltrometer). The good correlation between the K used in HYDRUS-3D to model the infiltration curves and those obtained by the NSH method (R^2 =0.98) indicates this technique is robust enough to estimate the soil hydraulic conductivity from complete infiltration curves. The numerical procedure to detect and remove the influence of the contact sand layer on the K and S estimates resulted to be robust and efficient. A negative effect of the curve infiltration noise on the K estimate was observed. The results showed that infiltration time was an important factor to estimate K. Smaller values of K or lower uncertainty required longer infiltration times. In a second step, the technique was tested in field conditions on 266 different soils at saturation conditions, using a 10 cm diameter disc infiltrometer. The NSH method was compared to the standard differentiated linearization procedure (DL), which estimates the hydraulic parameters using the simplified Haverkamp et al. (1994) equation, valid only for short to medium times. Compared to DL, NSH was considerably less affected by the infiltration bubbling and the contact sand layer, and allowed more robust estimates of K and S. Although comparable S values were obtained with both methods, the NSH technique, which is not limited to short times, resulted in more accurate and robust estimates for K. This paper

demonstrates the NSH method is a significant advance to estimate of the soil hydraulic properties from the transient water flow.

Keywords: Soil hydraulic properties; Sorptivity; Hydraulic conductivity; Cumulative infiltration; Contact sand layer; Transient water flow.

1. Introduction

In situ determination of soil hydraulic properties (sorptivity, *S*, and hydraulic conductivity, *K*) is a fundamental requirement of physically based models describing field infiltration and runoff processes. Over the last two decades, the tension disc infiltrometers (Perroux and White, 1988) have become popular devices for *in situ* estimates of K and S. This instrument consists of a disc base covered by a membrane, a graduated water-supply reservoir and a bubbling tower with a moveable air-entry tube that imposes the pressure head at the cloth base. The cumulative infiltration curve is measured from the water level drop in the reservoir. The diameter of the disc base can vary from the 25 cm proposed by Perroux and White (1988) to the 3.2 cm used by Madsen and Chandler (2007) for microtopography studies. Correct measurements of the water infiltration with the tension infiltrometer require the disc base to be completely in contact with the soil surface. To achieve this connection, Perroux and White (1988) recommended trimming any vegetation within the sample to ground level and covering the soil with a material with high hydraulic conductivity (contact sand layer). Although this procedure allows infiltration measurements in most field situations, the water initially stored in the contact layer alters the cumulative infiltration curve and, consequently, the estimation of K and S (Angulo-Jaramillo et al., 2000). In those cases, the influence of the contact layer should be removed. More recently, Sporgova et al. (2009) showed that the cumulative infiltration noise induced by the bubbling in the infiltrometer reservoir can have a significant effect on the K estimation.

The soil hydraulic properties are calculated by analysing the cumulative water-infiltration curve. Several methods to estimate the soil hydraulic properties have been proposed.: (i) methods based on the Wooding (1968) equation, which uses steady-state data (Smettem and Clothier, 1989; Ankeny et al., 1991; Reynolds and Elrick, 1991), (ii) methods based on the transient state data (e.g. Vandervaere et al., 2000) and (ii) methods which combine both transient and steady states, like BEST methods (Lassabatere et al., 2006; Yilmaz et al., 2010). Compared to the standard steady-state water flow method, the transient water flow procedure, that requires shorter experiments, involves smaller sampled soil volumes and more homogeneous initial water distribution (Angulo-Jaramillo et al., 2000), which leads to better estimates and better representativeness of the local hydraulic properties.

These are the reasons why we do not address steady state methods in this paper. Several model have been developed to estimate the soil hydraulic parameters from the transient water flow (Warrick and Broadbridge, 1992; Zhang, 1998). Haverkamp et al. (1994) obtained a quasi-exact equation describing the three-dimensional unsaturated cumulative infiltration curve for disc infiltrometers. Lassabatere et al. (2009) evaluated this equation with respect to their ability to reproduce numerically generated cumulative infiltration from 10 cm radius disc sources for four soils (sand, loam, silt and silty clay), and observed that the quasi-exact formulation was suitable for sand, loam and silt soils when their soil-dependent and saturation-independent shape parameters, γ and β, were properly chosen (between 0.75 and 1 and 0.3 and 1.7, respectively). Due to relative the complexity of this equation, Haverkamp et al. (1994) proposed a simplified version, which allows estimating K and S using linear fitting techniques. Vandervaere et al. (2000) compared the existing methods to analyse the transient state of the simplified Haverkamp et al. (1994) equation (for more details, see theory section). They concluded that the DL (for Derivative Linearization) method, which consists in a linear fit of a the derivative of the cumulative infiltration data with respect to the square root of time, allowed

1 the best estimations of K and S when contact sand layer was used. However, these methods,
2 like the DL method, are only applicable for short to medium time and can be questioned when
3 steady state is reached too quickly, e.g. when infiltration is controlled by capillary forces
4 (Angulo-Jaramillo et al., 2000).

5 This work proposes an inverse analysis of the complete Haverkamp et al. (1994) equation
6 (Numerical Solution of the Haverkamp equation, NSH) to estimate the soil hydraulic properties
7 from the cumulative infiltration curve measured with a disc infiltrometer. Due to the multiple
8 tension methods used in the infiltrometry technique require long infiltration measurements, and
9 the objective of this work is optimising the field measurements, only infiltration measurements
10 at saturation conditions were considered. This technique accounts for the effect of a sandy layer
11 embedded below the infiltrometer on cumulative infiltration, and removes its impact on
12 estimates. The procedure was validated with regards both analytically generated data and field
13 experiments for the case of water infiltration with zero pressure head at surface. At first, the
14 water infiltration was computed for the case of zero water pressure head at surface and dry
15 initial state for 12 different synthetic soils, using HYDRUS-2D. This numerical data were
16 analyzed with the NSH method and the estimated hydraulic values were compared to the
17 original ones. The effect of noise on data (e.g. due to air bubbling in the Mariotte reservoir of
18 the infiltrometer) and the consequences on the quality of NSH estimates were also numerically
19 assessed. In a second step, the NSH method was evaluated under field conditions and tested on
20 266 experimental infiltration curves. The results were compared to the DL procedure, which
21 can be considered as a reference method for the analysis of the transient state of infiltration.
22 The influence of the infiltration curves noise and the effect of the contact sand layer on the K
23 and S estimates was evaluated and discussed for all methods.
24

25 **2. Theory: Infiltration equation**

The 1-D cumulative infiltration, $I_{1D}(t)$, is described by the quasi-exact equation, derived by Haverkamp et al. (1990) from the Richards equation:

$$\frac{2(K_0 - K_n)^2}{S_0^2} t = \frac{2}{1-\beta} \frac{(K_0 - K_n)(I_{1D} - K_n t)}{S_0^2} -$$

$$\frac{1}{1-\beta} \cdot \ln\left[\frac{1}{\beta} \exp\left(2\beta(K_0 - K_n)(I_{1D} - K_n t)/S_0^2\right) + \frac{\beta - 1}{\beta}\right] \quad (1)$$

where S_0 is the sorptivity for θ_0; K_0 and K_n are the hydraulic conductivity values corresponding to θ_0 and θ_n, respectively; and β is defined as an integral shape parameter.

The 3-D cumulative infiltration, $I_{3D}(t)$, from a surface disc source can be expressed by the 1-D equation and an additional time linear term (Smettem et al., 1994):

$$I_{3D} = I_{1D} + \frac{\gamma S_0^2}{R_D(\theta_0 - \theta_n)} t \quad (2)$$

where R_D is the radius of the disc and γ is the proportionality constant. Substituting Eq.(2) into Eq.(1), the implicit 3-D infiltration equation is obtained (Haverkamp et al., 1990), valid for the entire time range:

$$\frac{2(K_0 - K_n)^2}{S_0^2} t = \frac{2}{1-\beta} \frac{(K_0 - K_n)\left[I_{3D} - K_n t - \gamma S_0^2 / \left((\theta_0 - \theta_n) R_D\right) t\right]}{S_0^2} -$$

$$\frac{1}{1-\beta} \cdot \ln\left[\frac{1}{\beta} \exp\left(2\beta(K_0 - K_n)\left[I_{3D} - K_n t - \gamma S_0^2 / \left((\theta_0 - \theta_n) R_D\right) t\right] / S_0^2\right) + \frac{\beta - 1}{\beta}\right] \quad (3)$$

This expression requires adequate values for the parameters γ and β. While in their earlier work, Haverkamp et al. (1994) proposed an average value of 0.75 for γ and 0.6 for β, Lassabatere et al. (2009) concluded that the shape parameters were closer to those predicted by Fuentes et al. (1992), especially for β. This study proved that Eq.(3) can describe cumulative infiltrations in sand, loam and silt soils but not for silty clay (a fine textured soil), due to its

hydraulic properties, which do not fulfil the conditions required for the validity of the quasi-exact formulation (see equations 2-4 in Lassabatere et al., 2009 for a detail of conditions to be fulfilled).

Haverkamp et al. (1994) established that, for short to medium time and assuming $K_n \to 0$, the 3D cumulative infiltration curve could be simplified to:

$$I_{3D} = S_0\sqrt{t} + \left[\frac{2-\beta}{3}K_0 + \frac{\gamma S_0^2}{R_D\left(\theta_n - \theta_0\right)}\right]t \tag{4}$$

which can be expressed as

$$I_{3D} = C_1\sqrt{t} + C_2 t \tag{5}$$

where

$$C_1 = S_0 \tag{6}$$

and

$$C_2 = \frac{2-\beta}{3}K_0 + \frac{\gamma S_0^2}{R_D\left(\theta_n - \theta_0\right)} \tag{7}$$

Applying the derivative operator to Eq.(4), the infiltration flux can be easily defined. In addition, the use algebraic combinations and the derivation with respect to the square root of time, lead to the following expression:

$$q_{3D} = C_1\frac{1}{2\sqrt{t}} + C_2 \tag{8}$$

$$\frac{I_{3D}}{\sqrt{t}} = C_1 + C_2\sqrt{t} \tag{9}$$

$$\frac{dI_{3D}}{d\sqrt{t}} = C_1 + 2C_2\sqrt{t} \tag{10}$$

The estimation of constants C_1 and C_2 is a prerequisite for the estimation of S_0 and K_0. To do so, different procedures can be employed: (i) fitting Eq. (4) to experimental cumulative infiltration; (ii) fitting Eq. (8) to the experimental infiltration rate; (iii) performing the linear

regression of the dataset ($t^{0.5}$,$I/t^{0.5}$), or finally, (iv) performing the linear regression of the dataset ($t^{0.5}$,$dI/dt^{0.5}$). These methods were referred to as CI for cumulative infiltration, IF for Infiltration Flux, CL for Cumulative Linearization and DL for Derivative Linearization (Vandervaere et al., 2000). According to these authors, only CL and DL technique allow revealing and eliminating the influence of the sand contact layer at the beginning of experiments. This effect can have negative effects on parameter estimations if not taken into account. Once C_1 and C_2 are known, S_0 and K_0 can easily be inferred using equations (6) and (7). It must be quoted that Eq.(4) is valid only for short to medium times, because it corresponds to a simplification of Eq.(3) developed under this assumption (Haverkamp et al., 1994). In this article, we focus on the DL method, which taking into account the short to medium infiltration time, is considered as a reference method for analysis of transient state infiltration data.

3. Material and methods

3.1. Numerical analysis

The numerical details of the proposed method are described in the following section. The approach is based on the Haverkamp et al. (1994) equation to describe the full-time cumulative infiltration curve. This equation does not have an explicit analytical solution and must be solved numerically resolving equation (3). The hydraulic parameters are then estimated fitting the theoretical curve to the experimental cumulative infiltration data. This process consists on a global optimization that explores the parameter space (S and K) looking for the best fit between the two curves, i.e. experimental data and implicit model. Details to account for the effect of the contact sand layer on the cumulative infiltration curve are also given. Finally, a sensitivity analysis was performed using the water level measurement as uncertainty source to account for the effect of the noise due to air bubbling in the reservoir

3.1.1. Numerical solution

In order to evaluate the 3-D cumulative infiltration equation, $I_{3D}(t)$, Eq.(3) must be solved by numerical analysis. Considering a single time value, *t*, and assuming known soil parameters, Eq.(3) can be rearranged as an infiltration function:

$$f(I) = 0 \tag{11}$$

The problem to solve $I_{3D}(t)$ is reduced to find the root of the $f(I)$ function. To this end, the simple and robust bisection method was used (Burden et al., 1985). The procedure defines an interval, $[I_1, I_2]$, where the function $f(I)$ takes opposite signs. The interval is then divided until the solution converges within a desired accuracy. To initiate the calculation, the start value for I_1 was set to zero and the initial value for I_2 was greater than the maximum expected infiltration. The algorithm was iteratively applied until a tolerance value (ε) of 10^{-3} was achieved:

$$I_2 - I_1 > \varepsilon \frac{I_1 + I_2}{2} \tag{12}$$

Large differences between nonlinear terms in Eq.(3) can lead to spurious solutions due to inaccurate results of fixed-precision arithmetic. To this end, the GMP (GNU Multiple Precision Arithmetic Library) library (Granlund, 2004) was used with 128 precision bits. Figure 1 shows an example of synthetic cumulative infiltration curves calculated for three of the studied synthetic soils (sand and loam and silt soils in Table 1).

3.1.2. Inverse analysis

Hydraulic parameters (sorptivity, S, and hydraulic conductivity, K) are estimated by minimizing an objective function, Q, that represents the difference between the implicit model Eq.(3) and the experimental cumulative infiltration data:

$$Q = \sum_{i=1}^{n} \left(\left(I_i - I\left(K, S, t_i\right) \right) \Delta t_i \right)^2 \quad (13)$$

where n is the number of measured (I,t) values. To this end, a brute-force search (Horst and Romeijn, 2002) was employed, enumerating all possible candidates of the hydraulic parameters to a certain precision and selecting the best result. This reference method, that requires considerable computing power, was used to study the properties of the solution space and lead to more efficient inverse methods. The γ and β values used in the analysis were fixed at their values by default i.e. 0.75 and 0.6, respectively (Haverkamp et al., 1994).

3.1.3. Sand-layer effect

To ensure contact between the soil and the disc base, a sand layer is commonly placed on the surface. However, the water stored in the sand influences the cumulative infiltration curve, contradicts the homogeneity assumption of Eq.(1) and invalids the hydraulic parameters obtained by the inverse analysis (Angulo-Jaramillo et al., 2000) (standard technique). A new procedure to omit the influence of the contact sand layer (layered flow analysis) on the K and S estimation is proposed. This consists of a layered flow model that assumes the water does not infiltrate into the soil until the sand layer is completely saturated. After this early stage, infiltration is assumed to occur as if the sand layer were inexistent with no flow impedance by the highly conductive sand. Under these assumptions, the effect of sand can be considered just as a delay of time and volume before water infiltration in the soil. Then, the effect of the contact layer can be removed by finding the sand infiltration time (and its corresponding water volume), that corresponds to the time required for water to fill in the sand, and shifting the experimental data to the origin (in time and water volume). To account for such a shift in infiltration time and volume, the proposed algorithm is based on the adaptation Eq.(13) to the layered flow problem as follows. For any set of infiltration data, several values are considered

for sand infiltration times and volumes, leading to the definition of a collection of infiltration curves as a function of sand infiltration and volume. Each curve is shifted in time and in volume before being analyzed through the minimization of the objective function, Eq. (13). This steps allows the selection of the hydraulic parameters that provide the best fitted. The corresponding curve and values for sand infiltration time and volume are selected. This approach captures the portion of the curve that best fits Eq.(3) and removes the sand layer effect. The range of the proposed infiltration sand time values was fixed between 0 and 5 seconds every 0.1 s.

3.1.4. Synthetic infiltration curves

Infiltration experiments were simulated using HYDRUS-3D model (Simunek et al., 1999), considering 12 different soils types (Table 1). Water retention curves were characterized using the van Genuchten (1980) model with Mualem condition. We considered the Mualem model for unsaturated hydraulic conductivity (Mualem, 1976). The soil volume was discretized as a cylinder (radius of 25 cm and depth of 25 cm), covering the axisymmetric plane with a 2-D rectangular mesh of 100×900 cells. The vertical cell size was variable to obtain more detail near the surface, ranging from 0.003 cm on the top to 0.3 cm on the bottom. Maximum and minimum time steps were fixed at 0.05 s and 10^{-4} s, respectively. Previous numerical analysis demonstrated that, under this discretization, the solution is grid independent.

A base disc infiltrometer of 10 cm radius was represented as a constant pressure head boundary on the corresponding cells, whereas the rest of the soil surface was treated as atmospheric boundary with no flux. A null pressure head was considered as bottom boundary. The lateral and the bottom boundaries of the soil cylinder were considered as no flux boundaries, condition that is valid if the water does not reach these regions. The initial soil water content was close to the residual water content to satisfy $\theta_n<0.25\ \theta_s$ that is required for

the validity of Eq.(1). The simulations run up to 50 mm water infiltration. This allowed obtaining a fixed precision in the soil hydraulic parameters estimation.

To validate the method that removes the influence of the contact layer, simulations were repeated on the same soils considering a 5 mm sand layer (with the same radius as the disc base) placed on the surface. These new numerical data were used for the inversion procedure using the layered flow option to assess the capability of the proposed procedure to find the sand infiltration time and volumes. Hydraulic properties of the contact sand layer are shown in Table 1.

3.1.5. Hydraulic stability

Air bubbling in the water reservoir can affect the measurement of the cumulative infiltration. To study the influence of air bubbling on the hydraulic parameter estimation, a synthetic noise was added to the synthetic infiltration curves calculated for the previous step (see above). A reference synthetic noise was extracted from the analysis of real experimental data used by Moret-Fernández et al. (2013a). To do so, the bubbling effect was extracted by comparing the experimental and the corresponding theoretical curves, fitted to Eq.(3) trough an inverse procedure. Statistical analysis of the difference between model and experimental data demonstrated that the resulting noise could be described by a normal distribution. Three increasing noise levels, corresponding to standard deviation values of 0.5, 1, and 2 mm, were incorporated to the simulated infiltration curves (Table 1). According to our experience with the disc infiltrometry technique, the selected standard deviation values cover most observed field conditions.

3.2. Field experiments

3.2.1. Experimental design

The NSH method was tested on experimental infiltration curves recorded in laboratory, two different sands (Table 2), and in semiarid dry lands of the central Ebro Basin (north-eastern Spain). The average annual precipitation of the experimental fields ranges between 313 and 350 mm and the average annual air temperature ranges between 13.3 and 14.5 ºC. The experimental fields were located in the municipalities of Peñaflor, Codo, Belchite, Leciñena, Sariñena and Bujaraloz. The lithology of the fields is gypseous alternating with non-gypseous areas. The traditional land use is an agro-pastoral system involving rainfed agriculture and extensive sheep grazing. The cropping system is a traditional cereal–fallow rotation, which involves a long fallow period of 16–18 months, running from June–July to November–December of the following year.

Five different contrasted soil managements were considered: ungrazed (NG) and grazed (GR) uncultivated lands, and cultivated soil under conventional (CT), reduce (RT) and no-tillage (NT) treatments. The NG and GR treatments were located on uncultivated soils at Leciñena, Belchite, Codo and Sariñena municipalities. The grazing intensity in the GR fields was < 1 livestock unit ha^{-1} $year^{-1}$. Natural vegetation cover is spatially discontinuous where vegetation is distributed in patches with wide open inter-patch areas. Measurements were performed on the bare soil of the inter-patch areas (Moret-Fernández et al. 2011). Agricultural fields were placed in Peñaflor and Bujaraloz. Experimental field in Peñaflor was located in the dryland research farm of the Estación Experimental de Aula Dei (CSIC) in the province of Zaragoza. The study was conducted on a large block of plots within a long-term conservation tillage experiment initiated in 1989. The field was in winter barley (*Hordeum vulgare L.*)-fallow crop system. Three different tillage treatments were examined: conventional tillage (CT), reduced tillage (RT) and no-tillage (NT). The CT and RT treatment consisted of mouldboard (40 cm depth) and chisel (30 cm depth) ploughing of fallow plots in early spring, respectively. NT used exclusively herbicides (glyphosate) for weed control throughout the

fallow season. All measurements were done in fallowed soils (F) and consisted of soils in the aggregation status after six to eight months of fallow, prior to any primary tillage operations. Details about the field characteristics of Peñaflor can be found in Moret and Arrúe (2007). Measurements in Bujaraloz were conducted on commercial agricultural fields under CT management. Three different soil structural conditions were considered: freshly moldboard tilled (MB), cropped (C) and fallowed soils. Infiltration measurements in MB were performed on freshly tilled soils just after a pass with a moldboard plow (in the spring of the 18-months fallow period), before any rainfall event. The C treatment corresponded to soils in the aggregation status for the last stages of winter cereal development (May–June). The soil under F did not present adventitious plants and was partially covered (>20%) with winter cereal crop residues. Measurements in C and F were performed between crop lines. A total of 16 sampling points under MB and C and 24 for F (Table 2) were selected in Bujaraloz. All measurements were conducted on nearly level areas (slope 0–2%) between February 2000 and April 2001, and February 2009 and October 2010. Details about the field characteristics of Bujaraloz can be found in Moret-Fernández et al. (2013c).

3.2.2. Soil hydraulic properties estimation from field measurements

All samplings for soil texture properties per experimental field were taken from the 0–10 cm depth soil layer. The samples, one replication per field, were homogenized and sieved up to 2mm for the subsequent laboratory analyses. The soil particle size distribution and related textural parameters were determined using the laser diffraction technique (COULTER LS230).

The soil dry bulk density (ρ_b) measured within the 2–7 cm depth soil layer, after removing the soil surface crust, was determined by the core method (Grossman and Reinsch, 2002) (50mm diameter and 50mm height). One replication was taken per infiltration measurements. The ρ_b values with mass water contents were subsequently used to determine the prior

volumetric water content and the saturated water contents needed to calculate the surface hydraulic conductivity K_0 using Mualem capillary model.

The transient cumulative infiltration curves were measured with a Perroux and White (1988) model tension disc infiltrometer. The diameter disc and internal diameter of the water reservoir tower was 100 mm and 34 mm, respectively. Two different base discs were used: (i) a conventional disc (C_{DB}) which base was covered with a tightened nylon cloth of 20-μm mesh and uses contact sand layer between the soil surface and the base disc; and (ii) a malleable base disc (M_{DB}), which base was covered with a loosened malleable nylon cloth of 20-μm mesh filled with 100 g of coarse sand (1–1.5 mm grain size; 0.5-cm-thick layer, approximately) (Moret-Fernádnez et al., 2013b). This alternative design allows adapting the base disc to the soil surface without using contact sand layer.

The infiltration measurements were taken on areas cleared of large clods and crop residue. These included infiltration measurements on the soil surface crust and on the 1–10 cm depth soil layer, after removing the surface crust (Table 2). For the conventional disc (C_{DB}) a thin layer (< 1 cm thick) of commercial sand (80–160 μm grain size and an air-entry value between -1 and -1.5 kPa), with the same diameter as the disc base, was poured onto the soil surface. The M_{DB} disc was directly placed on the soil surface. A total of 266 cumulative infiltration curves were recorded (Table 2). Measurements in Bujaraloz, Belchite, Codo, Leciñena and Sariñena were done with a C_{DB} disc, and infiltration measurements in Peñaflor with the C_{DB} and M_{DB} base (Table 2). All measurements were performed at 0 cm of pressure head. The water infiltration was measured from the drop of water level in the reservoir tower, which was automatically monitored with ±0.5 psi differential pressure transducer (PT) (Microswitch, Honeywell) (Casey and Derby, 2002). The scanning time interval was 10 seconds. Infiltration measurements lasted between 8 and 15 min. At the end of infiltration, a wet soil sample was taken to estimate the final gravimetric water content (W). The final volumetric water content

needed to estimate the soil hydraulic properties was calculated as the product between W and ρ_b.

The influence of the water reservoir bubbling on the DL and NSH methods was evaluated. To this end, four representative curves with different noise ranges, two with low and high noise, respectively, were selected. These correspond to infiltration experiments concluded in the Bujaraloz, Peñaflor and Codo fields (Table 4). The four infiltration measurements were conducted on the 1-10 cm depth soil layer, and contact sand layer was employed. In a second step, the influence of the contact sand layer on the DL and NSH methods was also studied.

The S and K estimated with the NSH method for the 266 measured field infiltration curves were subsequently compared to the corresponding values estimated with the DL procedure (when available). To prevent subjective decisions with DL, the following procedure was established:

(i) time interval of 10 s between two successive measures;

(ii) removal of the first points which correspond to water infiltration in the sand layer ;

(iii) total infiltration time was < 150 s.

Comparison between DL and NSH involved the following conditions:

(i) Eq.(10) curves with regression coefficients (R^2_{DL}) < 0.15 were omitted. The remaining curves (R^2_{DL} > 0.15) were grouped in three sets: (a) 0.15 > R^2_{DL} > 0.60, (b) 0.6> R^2_{DL} > 0.70 and (c) R^2_{DL} > 0.70

(ii) no negative K or S results were considered;

4. Results and discussion

4.1. Numerical analysis

4.1.1. Method validation

An excellent fitting was observed between synthetic and modelled cumulative infiltration curves for the case of infiltration with no sand layer (Fig. 2a; Table 3). The objective function presents a unique and narrow minimum around the optimal hydraulic properties values (Fig 2b and c). These results show that, for the case depicted in Figure 2, estimates can be properly identified for both sorptivity (S) and hydraulic conductivity (K), and that the estimates are close to the targeted values. Overall, NSH method provided accurate estimates for all cases. Estimated hydraulic conductivities and reference values present high correlation (R^2 = 0.95) (Fig. 3), indicating the ability of the method to estimate *K* from transient infiltration curves. Although Lassabatere et al. (2009) observed that the quasi-exact formulation was suitable when the soil-dependent and saturation-independent shape parameters, γ and β, are properly chosen, our results showed that the average values proposed by Haverkamp et al (1994) gave acceptable results.

As a second step, we inverted the data obtained for the layered profile (sand + soils) with the NSH method, based on the standard analysis without the layered flow analysis. We aimed at quantifying the impact of the sandy layer onto the quality of estimates in the case its negative effect is not considered. As showed in Figure 4, the first case concerns the inversion of synthetic cumulative infiltration obtained for the soil alone. The synthetic data are accurately fitted by the model and the estimates provided by the NSH –standard analysis method are accurate: $1.33 \cdot 10^{-2}$ versus $1.20 \cdot 10^{-2}$ m s^{-1} for saturated hydraulic conductivity. The embedment of the sand increase the cumulative infiltration (□ versus ○, in Figure 4).

The analysis of the synthetic cumulative infiltration with the NSH-standard analysis leads to a poor fit with underestimation of the data for short times. Related estimates are far from targeted values, specifically for the saturated hydraulic conductivity with a value of $4.37 \cdot 10^{-6}$ versus $1.20 \cdot 10^{-2}$ m s^{-1}. Finally, the use of layered flow analysis permits an accurate fit of the data (Figure 4) and give an appropriate value for estimates with $2.11 \cdot 10^{-2}$ versus $1.20 \cdot 10^{-2}$ m s^{-1}.

Similar results were obtained for the other cases. Inaccurate results are obtained when the standard analysis is applied to synthetic curves obtained for soils with contact sand layer (Fig. 3; Table 2). However, these errors vanished when the layered flow model is used (Fig. 3; Table 2), where a strong correlation ($R^2 = 0.93$) between the original and estimated *K* was observed (Fig. 3). These results show the NSH with layered flow analysis allows the use of infiltrometer with sand layer and a proper analysis of the data obtained in such configuration. These results validate the proposed method against synthetic data. For the case of soil 10, no results are available since the numerical calculation of water cumulative infiltration could not be determined, due HYDRUS numerical convergence errors.

4.1.2. Sensitivity and uncertainty

Infiltration measurements are affected by several sources of uncertainty (i.e. water level measurement, contact sand layer, effective disc radius, etc.), which may propagate its variability to the hydraulic parameters estimates. In our case, only the source of uncertainty due to water level measurement (±0.5 mm) was considered.

The water level measurement uncertainty depends on the reservoir diameter. Two different diameters (3.4 and 6.0 cm) were considered, resulting in increasing uncertainties for larger diameters (Fig. 5). A sensitivity analysis was performed, around each inverse solution, as part of a first order uncertainty analysis. The change of the objective function (Eq.13) associated to the uncertainty source was first calculated and transported to the inverse analysis parameter space, estimating the variability of the results (Fig. 5). It is clearly shown that larger water reservoir diameters result in an increase in measurement errors and thus widen the confidence intervals for all estimates (K and S). For this case, (soil #12, Figure 5), the confidence intervals are ($2.01 \cdot 10^{-2}$, $2.26 \cdot 10^{-2}$) and ($1.78 \cdot 10^{-2}$, $2.52 \cdot 10^{-2}$,mm s^{-1}), for K, respectively for a diameter of 6.0 and 3.4 cm. It can be noted while the range of confidence intervals are impacted, the

estimated values are not affected by this factor. Similar results were found for all the other soils.

The influence of the experiments duration on the estimates was also tested. Analysis of Eq.(3) showed that the accuracy of the hydraulic properties estimation depends also on the measurement time. Shorter infiltration times shift the optimal K values and widen the objective function. This is illustrated for the case of Soil #12 in Fig. 6. In this case, if we consider a desired precision in the measurements (here the same as for the infiltrometer with 3.4 cm in diameter), the change in time duration changes both the range of the confidence interval and the center of the interval (i.e. the estimation). Clearly, best estimates are obtained for longer experiments, which means that proper estimations for hydraulic conductivity and sorptivity require to wait long enough. The analysis was extended to all synthetic infiltration curves, to determine the minimum infiltration time required to estimate the hydraulic parameters within a certain relative accuracy (10 and 90%), by means of an iterative procedure (Fig. 7). The results show that: (i) infiltration time needed to estimate the hydraulic properties within a fixed uncertainty increases as the soil permeability decreases, and (ii) the S, which is mainly related to the initial infiltration times (Angulo-Jaramillo et al., 2000), is less affected than K by the infiltration time.

The NSH method appears interesting and promising since it uses the analytical expression developed by Haverkamp et al. (1994) that is valid for all times. Thus, opposite to other methods, this technique does not require the attainment of steady state, which can be quite time consuming for some soils. Yet, these calculations show that time duration of the dataset to be analyzed with the NSH method needs to be long enough. However, we consider that a constant water infiltration volume can be better criteria to obtain fixed accuracy for all soils. For a 10 cm diameter disc infiltrometer, we have found that this volume is about 50 mm.

4.1.3. Bubbling effect

A satisfactory fitting of the different noisy curves was observed (Fig. 8a). Although the objective function distribution around the optimal hydraulic properties values presents a unique minimal value, the noisiest curves tended to increase the width of the wells and, accordingly, the uncertainty of the estimations (Fig 8b and c), mostly for hydraulic conductivity (K). The results showed that S was not affected by the noise level (Fig. 9a). Only the noisiest infiltration curves had a significant influence on *K*, which optimal values differing from those calculated from the original curves (Fig. 9b). These results prove that the NSH method allows to treat even noisy data with no clear impact on the quality of estimates for both saturated hydraulic conductivity and sorptivity.

4.2. Field testing

4.2.1. Water reservoir bubbling influence

The bubbling in the water supply reservoir during the infiltration experiments, which perturbs the cumulative infiltration curves, had an important influence on the DL method. This method could be satisfactorily applied only on low noisy infiltration curves (Fig. 10a and b). In these cases, both DL and NSH procedures gave comparable K and S values (Table 4). Increasing noise in the infiltration curves (Fig. 10c.2 and d.2), reduced the R^2 related to Eq.(10) and prevented coherent estimates of K, which even gave negative values (Table 4). This problem, which is due to Eq.(10) is very sensitive to anomalous changes in the infiltration curve slopes, may be solved by increasing the infiltration time interval, smoothing the data, or removing spurious pair of $\frac{dI}{d\sqrt{t}}$ vs. $\sqrt{t}$ points. However, the subjectivity of this process, which depends on the researcher experience, makes the DL method to be time-consuming and subjective. This drawback of the DL method results from the derivation process which requires an extreme precision of the data. This problem vanished with NSH, with the use of the full-

time cumulative infiltration curve, is significantly less affected by the infiltration noise (Fig. 10.1). The low RMSEs between the NSH modelled and experimental curves (Table 4) indicate this method can satisfactorily be applied even in noisy infiltration curves. In addition, the values for estimates seem plausible.

4.2.2. Influence of the contact sand layer

The water initially stored in the contact sand layer during the early stages of the infiltration measurements makes a jump in the initial times of the cumulative infiltration curve (Fig. 10a and 2b). As reported by Vandervaere et al. (2000), this sand infiltration time (t_{sand}) should be removed from infiltration curve analysis to properly estimate the soil hydraulic properties. Applied on low-noisy infiltration curves, the DL method allowed revealing and removing the infiltration steps corresponding to the sand layer wetting (black points in Fig. 10.2). The remaining data could be satisfactorily used to estimate the K and S (Table 4). A completely different scenario was observed for noisy infiltration curves, where indistinguishable t_{sand} values were observed (Fig. 10c.2 and d.2). In these cases, the difficulty to detect t_{sand} and the subjectivity of this procedure makes the DL method to be inaccurate and uneasy to apply. These limitations vanish when using the NSH method (Fig. 10 and Table 4), which numerical approach automatically removes the t_{sand} infiltration steps and estimates K and S from the remaining cumulative infiltration values.

4.2.3. K and S estimates

Over the 266 experimental infiltration curves, a total of 158 measurements (59%), with a $R^2_{DL}<0.15$, were omitted from the DL analysis. Such percentage indicate a high rate of failure. From the remaining data, 87 curves (33%) presented a R^2_{DL} between 0.15 and 0.60, and only 21 measurements (8%) showed a $R^2_{DL} \geq 0.6$. These results indicate that only 40% of experimental

infiltration curves could be analysed by the DL method. Overall, the S estimated with DL was well correlated to that calculated with NSH (Fig. 11a). This is due to the high infiltration rates in the early infiltration stages providing accurate derivatives. A substantial worse K_{DL} vs K_{NSH} correlation was observed. Only linearized infiltration curves with $R^2_{DL} > 0.7$ gave a satisfactory K_{DL} vs K_{NSH} correlation ($R^2 = 0.96$) (Fig.11b). For the remaining measurements, a poorer K_{DL} vs K_{NSH} correlation was found, where DL tended to overestimate K. Two reasons could explain these results: (i) the DL method results are highly inaccurate for noisy infiltration curves ($R^2_{DL} < 0.6.$) (Fig. 10b); and (ii) the application of DL method is restricted to relatively short time (i.e. 150s). As above demonstrated, the selection of longer datasets with NSH method, that remain valid for all times, allows to increase the quality and accuracy of estimates and to reduce uncertainty. The analysis of time duration of the experiments on the estimates of K and S using the NSH method (Fig. 7) reveals that the infiltration time used in the field experiments (ranged between 480 and 900 s) was in most cases insufficient to estimate K and S with a 10% or 90% accuracy. In those cases, longer infiltration measurements should be recommended.

5. Conclusions

This paper describes, and evaluates under field conditions, a new numerical procedure (NSH) to estimate the soil K and S from the cumulative infiltration curve of a disc infiltrometer using the analytical equation developed by Haverkamp et al. (1994). This procedure also removes the effect of the contact sand layer to improve the quality of estimates for *K* and *S*. The method was satisfactorily validated on 12 synthetic infiltration curves simulated with HYDRUS-3D from known soil hydraulic properties, including scenarios with contact sand layer. A sensitivity analysis was conducted using the water level measurement as the source of uncertainty. The effect of the infiltration curve noise (due to the bubbling in the infiltrometer) and the minimum theoretical time to achieve accurate estimations were calculated and presented. The results

show that a constant water infiltration volume is a better criteria to obtain fixed accuracy for all soils. For a 10 cm diameter disc infiltrometer, we have found that this volume is about 50 mm. The method (NSH) was subsequently compared to the differential model (DL) on 266 infiltration measurements taken under different soil conditions. Compared to the DL procedure, NSH allowed more robust estimates of K and S, independently on the infiltration curve noise and the presence of contact sand layer between the soil surface and the base disc. The proposed method has the advantage to work with raw cumulative data, instead of differentiated data and to be valid for all times, which allow to consider large datasets. The results demonstrated that the NSH method means a substantial advance to estimate the soil hydraulic properties from transient water infiltration flows. However, new efforts should be done to include additional disc infiltrometer uncertainty sources, such as effective disc radius, in the analysis.

Acknowledgements

This research was supported by the Ministerio de Ciencia e Innovación of Spain (grant AGL2010-22050-C03-02) and by the Aragón regional government and La Caixa (Grants: 2012/ GA LC 074). We would like to thank to Oussama Mounzer for his technical help to develop this paper.

References

Angulo-Jaramillo R, Vandervaere JP, Roulier S, Thony JL, Gaudet JP, Vauclin, M. 2000. Field measurement of soil surface hydraulic properties by disc and ring infiltrometers. A review and recent developments. Soil Tillage Research 55: 1–29.

Ankeny, M.D., Ahmed, M., Kaspar, T.C., Horton, R., 1991. Simple field method determining unsaturated hydraulic conductivity. Soil Science Society of America Journal 55, 467-470.

Burden, R. L., Faires, J.D. 1985. Numerical Analysis (3rd ed.), PWS Publishers, ISBN 0-87150-857-5.

Casey FXM, Derby NE. 2002. Improved design for an automated tension infiltrometer. Soil Science Society of America Journal 66, 64–67.

Grossman, R. B., Reinsch, T. G. 2002. Bulk density and linear extensibility. *In*, Methods of Soil Analysis. Part 4, pp. 201–205, in J. H. Dane and G. C. Topp, eds., SSSA Book 360 Series No. 5. Soil Science Society of America, Madison WI.

Fuentes, C., Haverkamp, R., Parlange, J. Y. 1992. Parameter constraints on closed-form soil water relationships. Journal of Hydrology 134, 117-142.

Granlund, T. 2004. GNU MP: The GNU Multiple Precision Arithmetic Library, 4.1.4 ed. http://gmplib.org/.

Haverkamp, R., Parlange, J.Y., Starr, J.L., Schmitz, G., Fuentes C. 1990, Infiltration under ponded conditions: 3. A predictive equation based on physical parameters. Soil Science 149, 292–300.

Haverkamp R, Ross PJ, Smettem KRJ, Parlange JY. 1994. Three dimensional analysis of infiltration from the disc infiltrometer. Part 2. Physically based infiltration equation. Water Resources Research 30: 2931-2935.

Horst, R., Romeijn, H. E. (Eds.). 2002. Handbook of global optimization (Vol. 2). Springer Science & Business Media.

Kodesová, R., Jirku, V., Kodes, V., Mühlhanselová, M., Nikodem, A., Zigova, A. 2011. Soil structure and soil hydraulic properties of Haplic Luvisol used as arable land and grassland. Soil and Tillage Research 111, 154–161.

Lassabatere L., Angulo-Jaramillo R., Soria Ugalde J. M., Cuenca R., Braud I., Haverkamp, R. 2006. Beerkan Estimation of Soil Transfer parameters through infiltration experiments – BEST. Soil Science Society of America Journal, 70, 521-532.

Lassabatere, L., Angulo-Jaramillo, R., Soria-Ugalde, J.M., Simunek, J. Haverkamp, R. 2009. Numerical evaluation of a set of analytical infiltration equations. Water Resources Research, 45, doi:10.1029/2009WR007941.

Madsen, M.D., Chandler, D.G. 2007. Automation and use of mini disk infiltrometers. Soil Science Society of America Journal 71, 1469-1472.

Moret, D., Braud, I., Arrúe, J.L. 2007. Water balance simulation of a dryland soil during fallow under conventional and conservation tillage in semiarid Aragon, Northeast Spain. Soil and Tillage Research 92, 251–263.

Moret-Fernández, D., Bueno, G., Pueyo, Y., Alados, C.L. 2011. Hydro-physical responses of gypseous and non-gypseous soils to livestock grazing in a semi-arid region of NE Spain. Agricultural Water Management 98, 1822-1827.

Moret-Fernández, Latorre, B., González-Cebolada, C. 2013a. Microflowmeter–tension disc infiltrometer: Part II – Hydraulic properties estimation from transient infiltration rate analysis. Journal of Hydrology 466-467, 159-166.

Moret-Fernández , D., Blanco, N., Martínez-Chueca , V., Bielsa, A. 2013b. Malleable disc base for direct infiltration measurements using the tension infiltrometry technique. Hydrological Processes 27, 275-283.

Moret-Fernández, D., Castañeda, C., Paracuellos, E., Jiménez. S., Herrero, J. 2013c. Hydro-physical characterization of contrasting soils in a semiarid zone of the Ebro river valley (NE Spain). Journal of Hydrology 486, 403-411.

Perroux KM, White I. 1988. Designs for disc permeameters. Soil Science Society of America Journal 52, 1205–1215.

Reynolds, W.D., Elrick, D.E., 1991. Determination of hydraulic conductivity using a tension infiltrometer. Soil Science Society of America Journal 55, 633–639.

Šimunek, J., Šejna, M., van Genuchten, M-Th. 1999. The HYDRUS-2D software package for simulating the two-dimensional movement of water, heat, and multiple solutes in variably-saturated media. Version 2.0. U.S. Salinity laboratory, Agricultural Research Service, USDA, Riverside, California.

Špongrová, K., Kechavarzi, C., Dresser, M., Matula, S., Godwin, R.J. 2009. Development of an automated tension infiltrometer for field use. Vadose Zone Journal 8, 810-817.

Špongrová, K., Matula, S., Kechavarzi, C., Dresser, M. 2010. Differences in topsoil properties of a sandy loam soil under different tillage treatments. 19th World Congress of Soil Science, Soil Solutions for a Changing World. Brisbane, Australia.

Smettem, K.R.J., Clothier, B.E., 1989. Measuring unsaturated sorptivity and hydraulic conductivity using multi-disc permeameters. Journal of Soil Science 40, 563-568.

Smettem, K.R.J., Parlange, J.Y., Ross, P.J., Haverkamp, R., 1994. Three-dimensional analysis of infiltration from the disc infiltrometer. Part 1. A capillary-based theory. Water Resources Research 30, 2925-2929.

Vandervaere, J.P., Vauclin, M., Elrick, D.E., 2000. Transient Flow from Tension Infiltrometers. Part 1. The two-parameter Equation. Soil Science Society of America Journal 64, 1263-1272.

van Genuchten, M.T. 1980. A closed form equation for predicting the hydraulic conductivity of unsaturated soils. Soil Science Society of America Journal 44, 892– 898.

Warrick, A.W., Broadbridge, P., 1992. Sorptivity and macroscopic capillary length relationships. Water Resources Research 28, 427-431.

Wooding, R.A., 1968. Steady infiltration from a shallow circular pond. Water Resources Research 4, 1259-1273.

Yilmaz D., Lassabatere L., Angulo R., Legret M. 2010. Hydrodynamic characterization of BOF slags through adapted BEST method. Vadoze Zone Journal, 9 (1), 107-116.

Zhang, R. 1998. Estimating soil hydraulic conductivity and macroscopic capillary length from disc infiltrometer. Soil Science Society of America Journal 62, 1513-1521.

Figures captions

Figure 1. Synthetic cumulative infiltration curves for sand, loam and silt soils (Table 1)

Figure 2. (a) Synthetic infiltration curve (circles) for a loam soil under no tillage treatment (Table 1; soil 12) and the corresponding fitted Eq.(3) curve (line), without contact sand layer, and the objective function distribution around the optimal values for (b) S and (c) K.

Figure 3. Correlation between the proposed *K* values (Table 1) and the estimations using Eq.(3) for the following scenarios: (○) NSH inversion of synthetic cumulative infiltrations into soils without sand layer and standard analysis, (□) NSH inversion of synthetic cumulative infiltrations into soils with sand layer and standard technique and (△)NSH inversion of synthetic cumulative infiltrations into soils with sand layer and layered flow analysis.

Figure 4. Synthetic curve for soil 12 (Table 1) and the corresponding fitted curves for the following scenarios: synthetic cumulative infiltration for the soil without sand layer (○) and standard analysis (–),synthetic cumulative infiltration for the soil with sand layer (□) analysed with the NSH standard technique (– · –) and or with NSH with layered flow analysis (––). Black squares correspond to the estimated initial sand layer infiltration.

Figure 5. Estimation of the uncertainty for S and K estimations considering soil 12, two diameter reservoir of 3.4 and 6.0 mm.

Figure 6. Objective function distribution around the optimal values for S and K considering soil 12 and infiltration times of 700 s (continuous line) and 100 s (discontinuous line).

Figure 7. Required infiltration time to estimate the hydraulic parameters within a relative accuracy of 10 and 90%, considering a water level error source (±0.5 mm) applied to a 1.6 cm diameter reservoir. Colours and contour levels denote the required infiltration time in (base-10) logarithm seconds time, and K and S are plotted in (base-10) logarithm scale.

Figure 8. Synthetic curves for soil 12 (Table 1) with three noise levels (normal distributions with standard deviation of 0 (○), 0.5 (△), 1 (□), and 2 (◊) mm) and fitted cumulative infiltration (a) and objective functions distribution around the optimal values for S (b) and K (c).

Figure 9. Correlation between the original *K* (a) and S (b) values (Table 1) and the estimations considering different noise level (normal distributions with standard deviation of 0.5 (△), 1 (□), and 2 (◊) mm). Error bars denote the uncertainty of the different results.

Figure 10. **a.1 to d.1**) Comparison between cumulative infiltration curves measured (points) in four different fields (Table 2), and the corresponding 3D modelled curves simulated from the hydraulic properties (Table 2) estimated with the DL (black discontinuous line) and NSH (grey continuous line) methods; and **a.2 to d.2**) the DL method applied to the corresponding soils. Black points denote the section of the linear fitting curve corresponding to the contact sand layer.

Figure 11. Relationship between the soil sorptivity (S) (a) and hydraulic conductivity (K) (b) estimated with the DL and NSH methods. Circles (○), triangles (△) and squares (□) denote comparison between DL and NSH for $R^2_{DL} > 0.7$, $0.6 > R^2_{DL} > 0.7$, and $0.15 > R^2_{DL} > 0.6$, respectively.

Table 1. Synthetic soils considered for the numerical study: soil textures, conditions and hydraulic parameters used in the HYDRUS-3D simulations.

Soil number	Soil texture	Soil conditions	θ_s	θ_{res}	α (cm)	n	K_s (mm s^{-1})	Reference
1	Sand	Sieved soil	0.43	0.04	0.145	2.68	$8.25\ 10^{-2}$	Lassabatere et al. (2009)
2	Loam	Sieved soil	0.43	0.08	0.036	1.56	$2.88\ 10^{-3}$	Lassabatere et al. (2009)
3	Silt	Sieved soil	0.46	0.03	0.016	1.37	$6.95\ 10^{-4}$	Lassabatere et al. (2009)
4	Silty clay loam	Arable soil; Horizon Bt1	0.41	0.27	0.051	1.53	$9.36\ 10^{-3}$	Kodesová et al. (2011)
5	Silty loam	Arable soil; Horizon C	0.38	0.01	0.026	1.18	$4.52\ 10^{-3}$	Kodesová et al. (2011)
6	Silty loam	Grassland; Horizon A2	0.49	0.19	0.088	1.24	$8.18\ 10^{-3}$	Kodesová et al. (2011)
7	Sandy loam soil	Conventional tillage	0.35	0.05	0.169	1.46	$6.98\ 10^{-2}$	Špongrová et al. (2010)
8	Sandy loam soil	Direct drill	0.38	0.05	0.192	1.46	$8.35\ 10^{-2}$	Špongrová et al. (2010)
9	Sandy loam soil	Conventional tillage wheel mark	0.36	0.05	0.110	1.68	$3.90\ 10^{-2}$	Špongrová et al. (2010)
10	Loam soil	Conventional tillage	0.49	0.06	0.100	2.25	$3.00\ 10^{-2}$	Moret et al. (2007)
11	Loam soil	Reduce tillage	0.49	0.07	0.091	2.24	$2.10\ 10^{-2}$	Moret et al. (2007)
12	Loam soil	No tillage	0.42	0.09	0.033	2.21	$1.20\ 10^{-2}$	Moret et al. (2007)

Table 2. Location, soil type, textural classification (USDA), soil management and number of infiltration measurements conducted in the different experimental fields.

Field	Soil	Textural classification	Soil status [1]	Treatments [2]	Nº of infiltration measurements			
					On SC [3] with CSL [4]	On SC without CSL	On 0-10 layer with CSL	On 0-10 layer without CSL
Laboratory		Sand (250-500 μm)			-	-	-	1
Laboratory		Sand (80-160 μm)			-	-	-	1
Peñaflor	Non-Gypseus	Loam soil	F	CT, RT, NT	9	9	9	9
Bujalaloz	Gypseous	Sandy loam to clay loam	F, C, MB	CT	24	-	40	-
	Non-gypseous	Loam to silty clay loam	F, C, MB	CT	22	-	37	-
Belchite	Gypseous	Sandy loam	N	NG	8	-	8	-
		Sandy loam	N	GR	12	-	12	-
Leciñena	Gypseous	Sandy loam	N	NG	4	-	4	-
		Sandy loam	N	GR	8	-	8	-
Sariñena	Non-gypseous	Sandy loam	N	NG	5	-	5	-
		Loam	N	GR	7	-	8	-
Codo	Non-gypseous	Loam	N	GR	8	-	8	-

[1] MB, F and C are freshly mouldboard tilled, cropped and fallowed cultivated soils, respectively, and N means uncultivated soil
[2] CT, RT and NT are conventional, reduce and no tillage treatment, and NG and G are ungrazed and grazed soils, respectively.
[3] Surface crust.
[4] Contact sand layer between disc base and soil surface.

Table 3. Hydraulic parameters estimated from synthetic infiltration curves and objective function (Q) for the following scenarios: (a) inversion of synthetic data for soils without sand layer and using NSH standard analysis, (b) inversion of synthetic data for soils with sand layer using NSH standard analysis and (c) inversion of synthetic data for soils with sand layer using NSH with layered flow analysis.

Soil nº		Scenario (a)		Scenario (b)		Scenario (c)	
		Average [Confidence interval] [1]	Q	Average [Confidence interval]	Q	Average [Confidence interval]	Q
1	S (mm $s^{-0.5}$)	1.50 e+00 [1.50 e+00, 1.51 e+00]	3.19 e-02	-	-	-	-
	K (mm s^{-1})	1.00 e-01 [9.92 e-02, 1.01 e-01]					
2	S (mm $s^{-0.5}$)	3.66 e-01 [3.66 e-01, 3.67 e-01]	3.65 e-02	4.10 e-01 [4.10e-01, 4.11e-01]	2.59 e-01	3.49 e-01 [3.47 e-01, 3.50 e-01]	7.28 e-03
	K (mm s^{-1})	2.09 e-03 [2.05 e-03, 2.14 e-03]		1.91 e-05 [-2.91 e-04, 1.14 e-04]		2.82 e-03 [2.73 e-03, 2.90 e-03]	
3	S (mm $s^{-0.5}$)	2.39 e-01 [2.39 e-01, 2.40 e-01]	2.93 e-02	2.57 e-01 [2.56 e-01, 2.57 e-01]	5.21 e-01	2.35 e-01 [2.34 e-01, 2.35 e-01]	5.39 e-03
	K (mm s^{-1})	2.57 e-04 [2.38 e-04, 2.77 e-04]		3.20 e-06 [1.00e -05, 5.37 e-05]		4.17 e-04 [3.84 e-04, 4.52 e-04]	
4	S (mm $s^{-0.5}$)	2.87 e-01 [2.86 e-01, 2.87 e-01]	3.56 e-02	3.82 e-01 [3.81 e-01, 3.83 e-01]	2.42 e-01	3.16 e-01 [3.14 e-01, 3.17 e-01]	1.05 e-02
	K (mm s^{-1})	9.12 e-03 [9.07 e-03, 9.20 e-03]		5.01 e-03 [4.91 e-03, 5.16 e-03]		9.33 e-03 [9.20 e-03, 9.47 e-03]	
5	S (mm $s^{-0.5}$)	2.27 e-01 [2.27 e-01, 2.28 e-01]	1.39 e-01	3.05 e-01 [3.04 e-01, 3.06 e-01]	2.91 e-01	2.48 e-01 [2.46 e-01, 2.49 e-01]	8.29 e-03
	K (mm s^{-1})	3.47 e-03 [3.45 e-03, 3.49 e-03]		2.99 e-03 [2.95 e-03, 3.05 e-03]		4.37 e-03 [4.31 e-03, 4.42 e-03]	
6	S (mm $s^{-0.5}$)	2.11 e-01 [2.00 e-01, 2.13 e-01]	4.92 e-01	2.90e-01 [2.89 e-01, 2.91 e-01]	2.14 e-01	2.43 e-01 [2.41e-01, 2.45e-01]	1.29 e-02
	K (mm s^{-1})	6.61 e-03 [6.54 e-03, 6.63 e-03]		7.24 e-03 [7.21 e-03, 7.32 e-03]		8.13 e-03 [8.06 e-03, 8.20 e-03]	
7	S (mm $s^{-0.5}$)	6.41 e-01 [6.37 e-01, 6.46 e-01]	1.76 e-01	6.66 e-01 [6.63 e-01, 6.69 e-01]	1.37 e-01	6.30 e-01 [6.14 e-01, 6.44 e-01]	1.76 e-01
	K (mm s^{-1})	6.03 e-02 [6.00 e-02, 6.07 e-02]		6.03 e-02 [6.00 e-02, 6.05 e-02]		5.89 e-02 [5.81 e-02, 5.96 e-02]	
8	S (mm $s^{-0.5}$)	7.13 e-01 [7.04 e-01, 7.19 e-01]	2.81 e-01	7.08 e-01 [7.05 e-01, 7.14 e-01]	1.11 e-01	6.75 e-01 [6.54 e-01, 6.88 e-01]	1.95 e-01
	K (mm s^{-1})	7.08 e-02 [7.04 e-02, 7.13 e-02]		6.61 e-02 [6.58 e-02, 6.64 e-02]		6.46 e-02 [6.38 e-02, 6.55 e-02]	
9	S (mm $s^{-0.5}$)	7.70 e-01 [7.68 e-01, 7.72 e-01]	4.90 e-02	7.06 e-01 [7.01 e-01, 7.10 e-01]	1.04 e-02	7.06 e-01 [7.01 e-01, 7.10 e-01]	1.04 e-02
	K (mm s^{-1})	3.39 e-02 [3.36 e-02, 3.42 e-02]		3.89 e-02 [3.84 e-02, 3.94 e-02]		3.89 e-02 [3.84 e-02, 3.94 e-02]	
10	S (mm $s^{-0.5}$)	3.45 e+00 [3.44 e+00, 3.45 e+00]	1.89 e-02	-	-	-	-
	K (mm s^{-1})	2.82 e-02 [2.44 e-02, 3.21 e-02]					
11	S (mm $s^{-0.5}$)	9.27 e-01 [9.25 e-01, 9.30 e-01]	3.93 e-02	1.04 e+00 [1.03 e+00, 1.04 e+00]	1.70 e-01	9.02 e-01 [8.98 e-01, 9.07 e-01]	1.95 e-01
	K (mm s^{-1})	2.34 e-02 [2.32 e-02, 2.38 e-02]		1.35 e-02 [1.31 e-02, 1.41 e-02]		6.46 e-02 [6.38 e-02, 6.55 e-02]	
12	S (mm $s^{-0.5}$)	1.03 e+00 [1.03 e+00, 1.03 e+00]	3.67 e-02	1.11 e+00 [1.11 e+00, 1.12 e+00]	1.74 e-01	9.57 e-01 [9.53 e-01, 9.61 e-01]	1.07 e-02
	K (mm s^{-1})	1.33 e-02 [1.29 e-02, 1.39 e-02]		4.37 e-06 [1.00 e-05, 6.31 e-04]		2.11 e-02 [2.05 e-02, 2.20 e-02]	

[1] Confidence interval estimated considering uncertainty due to water level measurement (±0.5 mm) for a 1.6 cm diameter reservoir.

Table 4. Soil sorptivity (S) and hydraulic conductivity (K) estimated with a 10 cm diameter disc infiltrometer in four different fields in Bujaraloz, Peñaflor and Codo with the DL and the NSH methods. Q and t_{sand} denotes the objective function (Eq. 13) and the time to saturate the contact sand layer, respectively. Within square bracket, the average confidence interval estimated with NSH considering uncertainty due to water level measurement (±0.5 mm) for a 1.6 cm diameter reservoir.

Location	Field	DL				NSH			
		S (mm s^{-05})	K (mm s^{-1})	R^2	t_{sand} (s)	S (mm s^{-05})	K (mm s^{-1})	Q	t_{sand} (s)
Bujaraloz	CAL006_NC_R_1	0.51	0.0428	0.81	10-15	0.43 [0.422-0.431]	0.0422 [0.0418-0.0426]	0.091	4
Peñaflor	SD_1_MF	0.29	0.0270	0.22	5-10	0.36 [0.359-0.366]	0.0110 [0.0103-0.0116]	0.069	2
Codo	Plan_ past_NC_R_8	1.26	-0.2431	0.12	5-10	0.34 [0.339-0.348]	0.0007 [0.0001-0.001]	0.150	5
Bujaraloz	03_NC_R2	1.04	-0.0079	0.03	5-10	0.64 [0.637 0.644]	0.0083 [0.0072-0.0097]	0.570	4

[1]

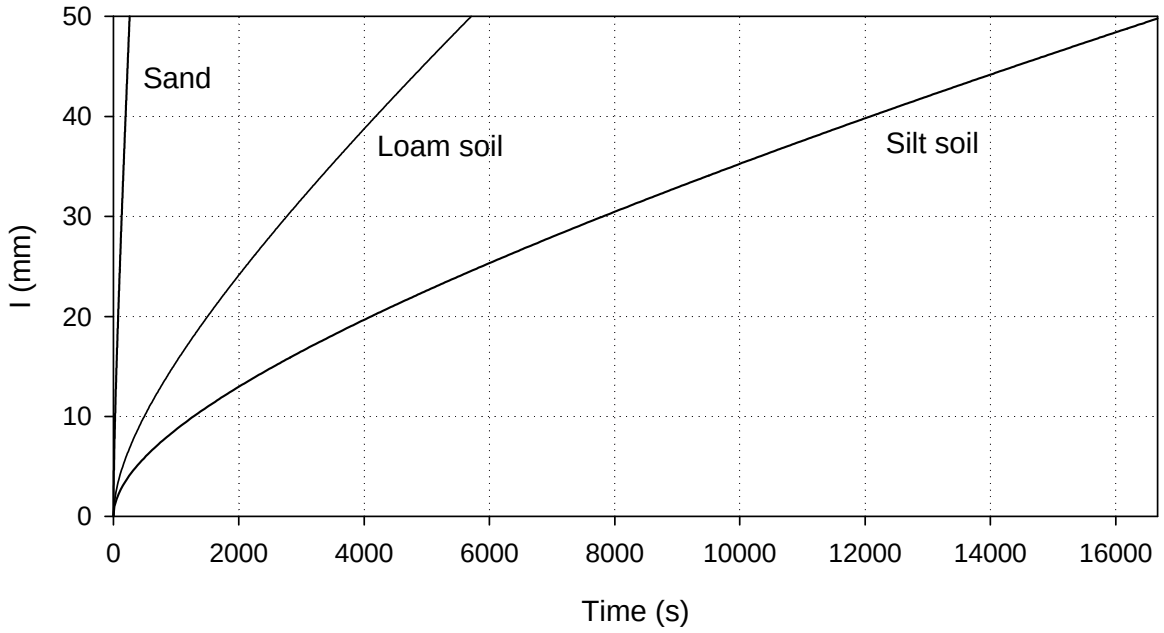
Sand
Loam soil
Silt soil
I (mm)
Time (s)
0
10
20
30
40
50
0
2000
4000
6000
8000
10000
12000
14000
16000

Figure 1.

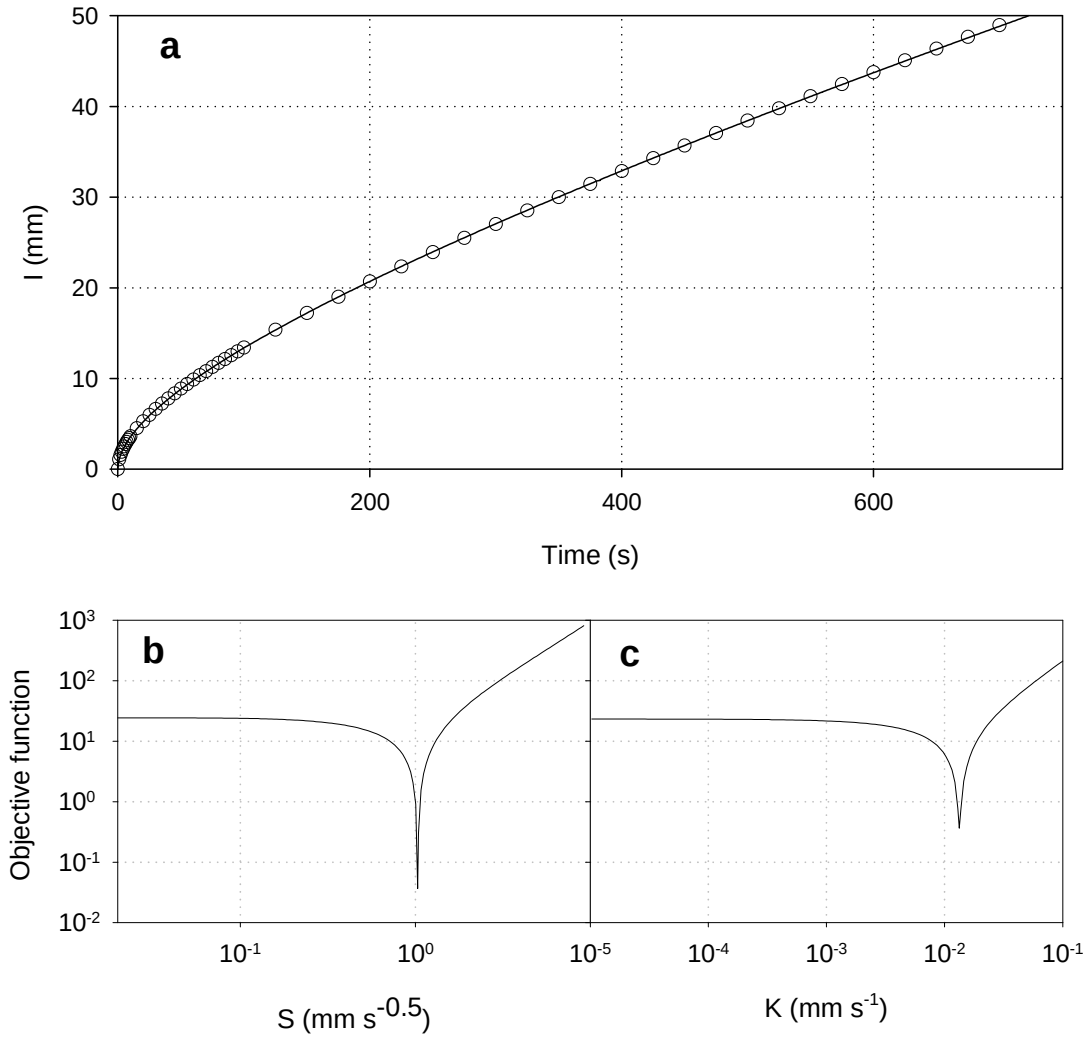
a
I (mm)
Time (s)
0
10
20
30
40
50
0
200
400
600
b
c
Objective function
10^{3}
10^{2}
10^{1}
10^{0}
10^{-1}
10^{-2}
10^{-1}
10^{0}
10^{-5}
10^{-4}
10^{-3}
10^{-2}
10^{-1}
S (mm $s^{-0.5}$)
K (mm s^{-1})

Figure 2.

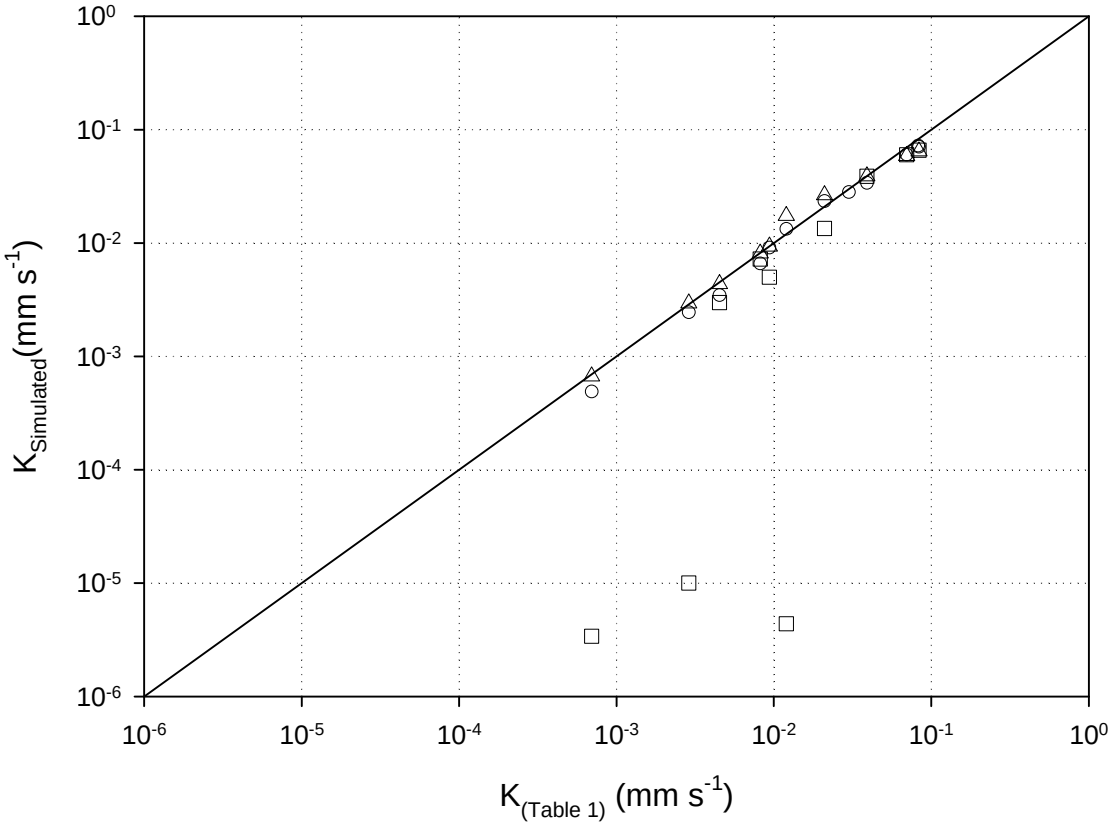
10^{0}
10^{-1}
10^{-2}
10^{-3}
10^{-4}
10^{-5}
10^{-6}
$K_{Simulated}$(mm s^{-1})
10^{-6}
10^{-5}
10^{-4}
10^{-3}
10^{-2}
10^{-1}
10^{0}
$K_{(Table\ 1)}$ (mm s^{-1})

Figure 3.

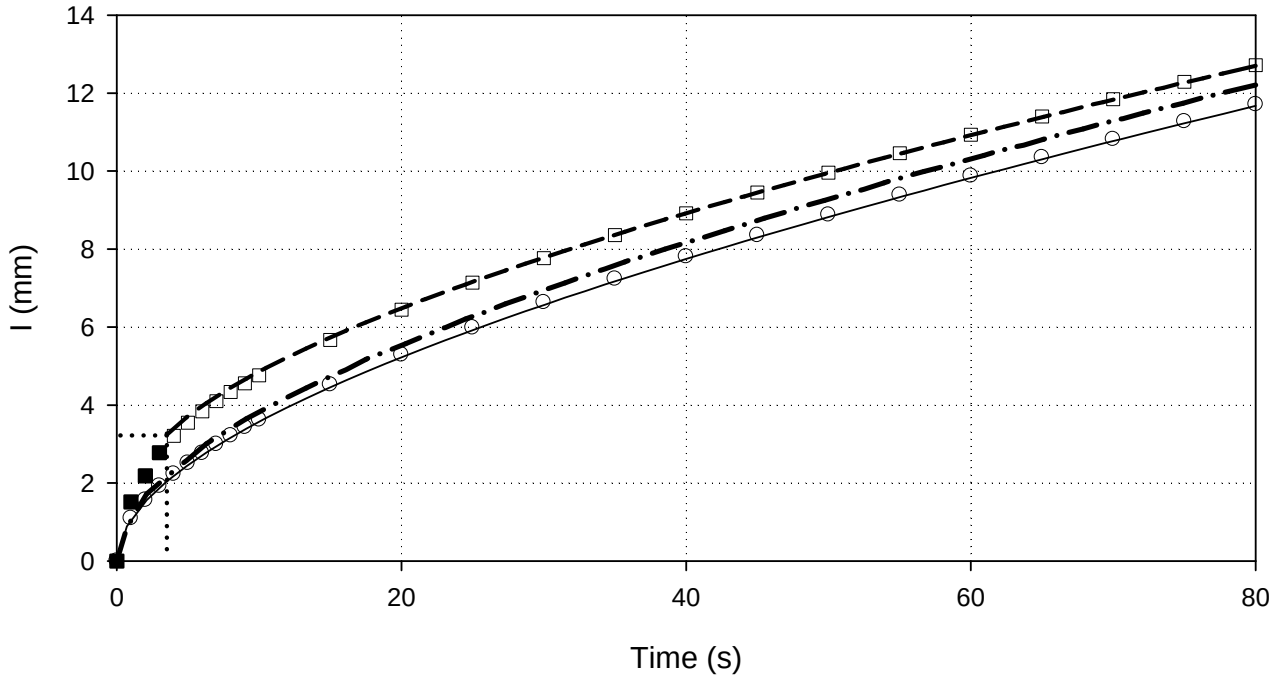

Figure 4.

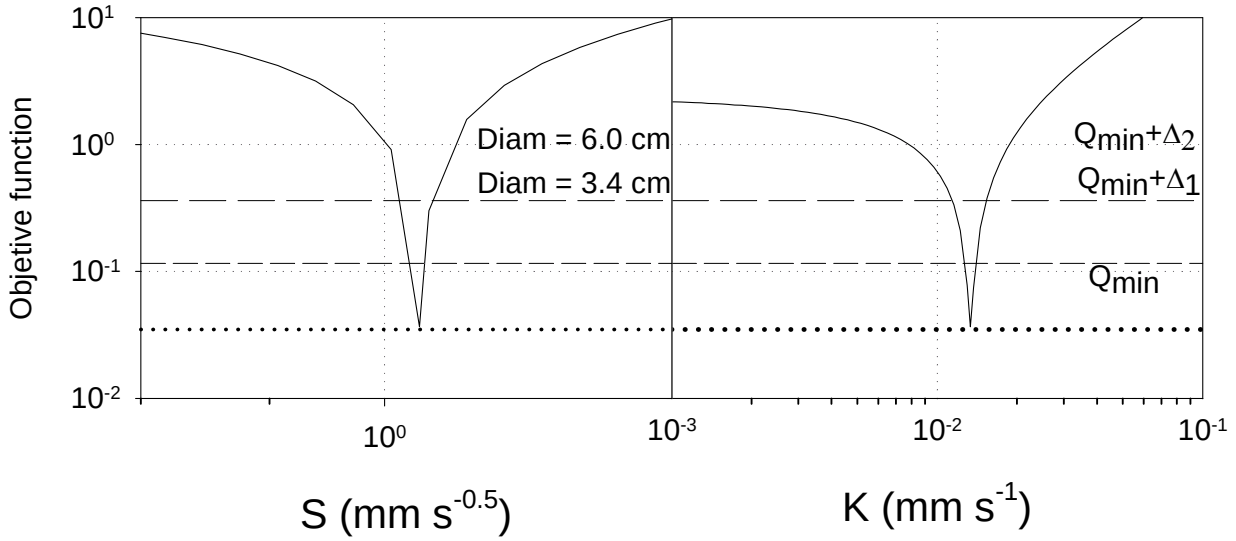
Objetive function
10^1
10^0
10^-1
10^-2
Diam = 6.0 cm
Diam = 3.4 cm
Qmin+Δ2
Qmin+Δ1
Qmin
10^0
10^-3
10^-2
10^-1
S (mm s^-0.5)
K (mm s^-1)

Figure 5.

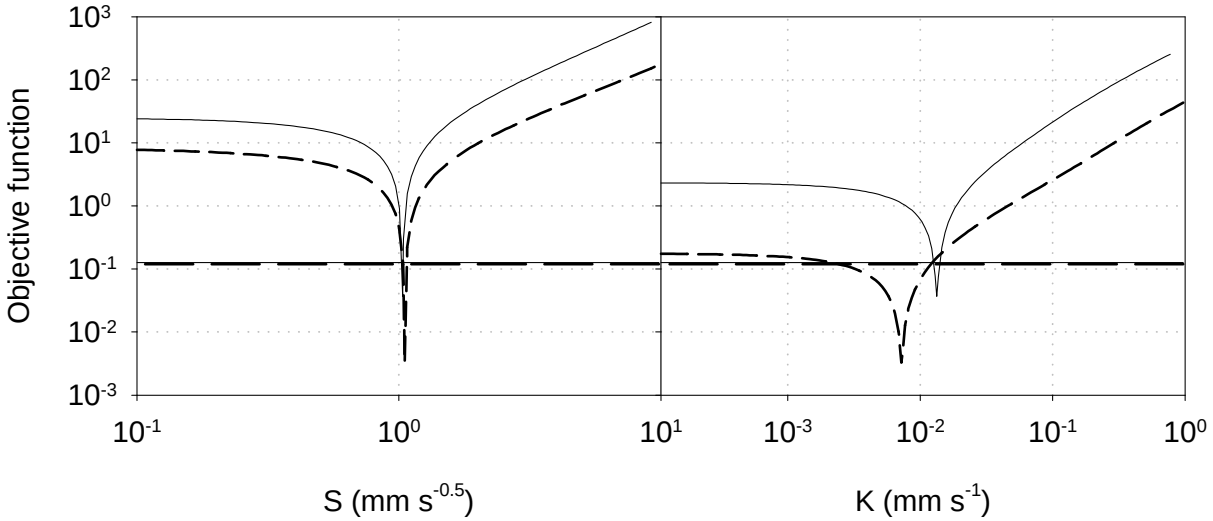
Objective function
10^3
10^2
10^1
10^0
10^-1
10^-2
10^-3
10^-1
10^0
10^1
10^-3
10^-2
10^-1
10^0
S (mm s^-0.5)
K (mm s^-1)

Figure 6.

a

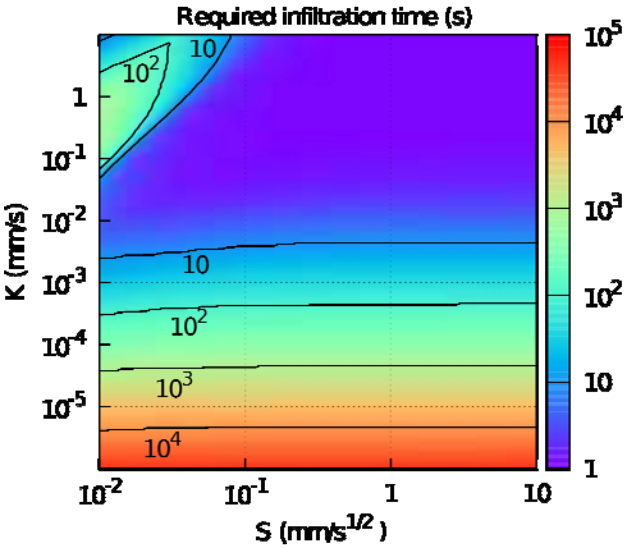
Required infiltration time (s)
K (mm/s)
S (mm/s^1/2)
10
10^2
10^3
10^4
10^5
1
10^-1
10^-2
10^-3
10^-4
10^-5

b

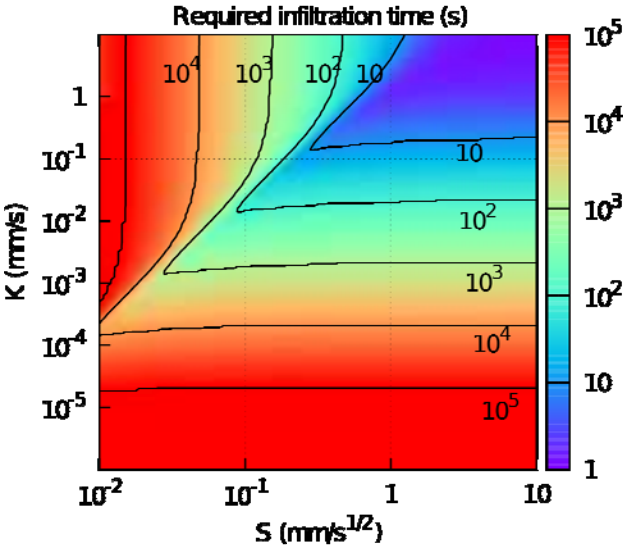
Required infiltration time (s)
K (mm/s)
S (mm/s^1/2)
10
10^2
10^3
10^4
10^5
1
10^-1
10^-2
10^-3
10^-4
10^-5

Figure 7.

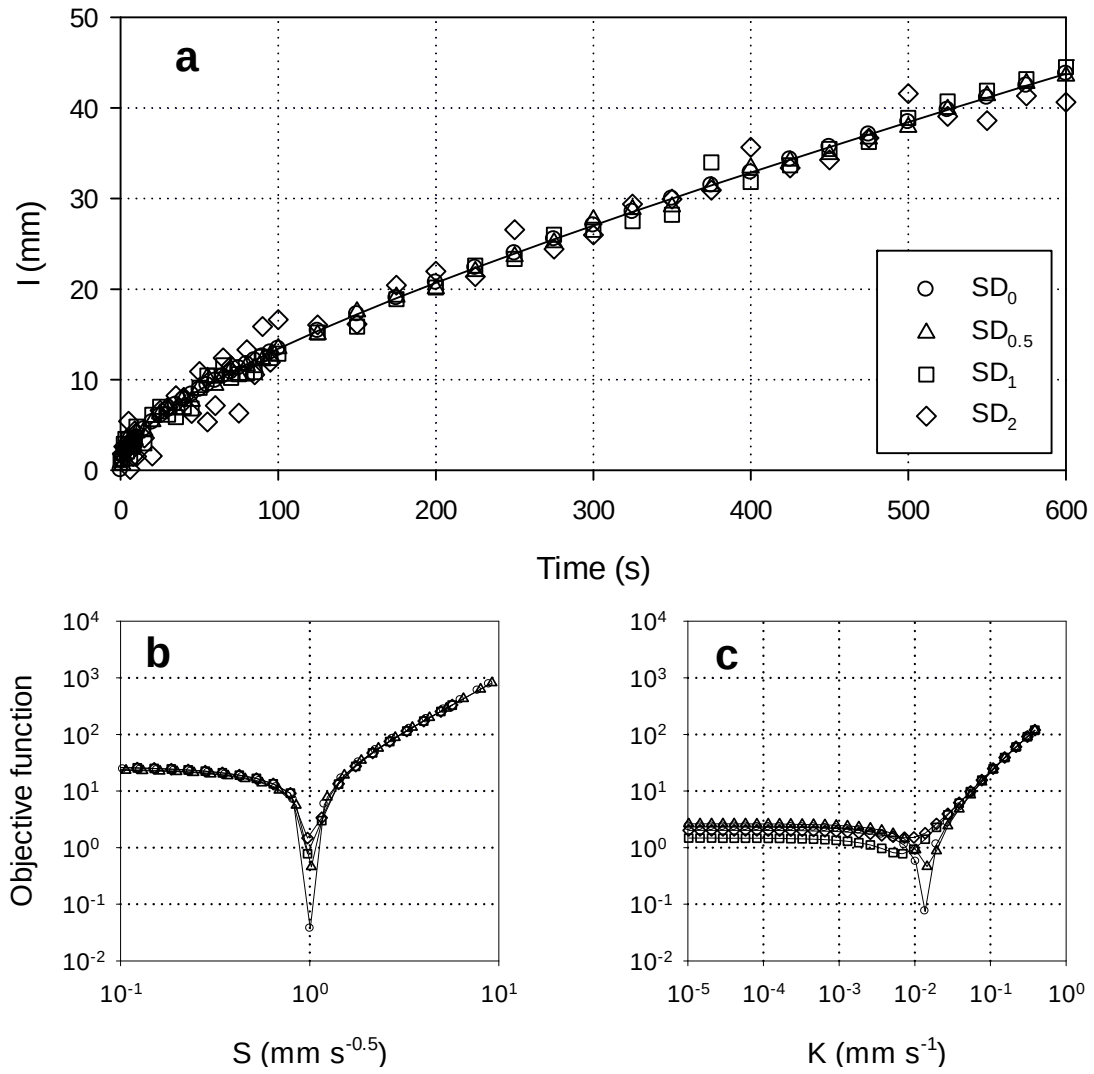
a
I (mm)
Time (s)
SD0
SD0.5
SD1
SD2
b
Objective function
S (mm s-0.5)
c
K (mm s-1)

Figure 8.

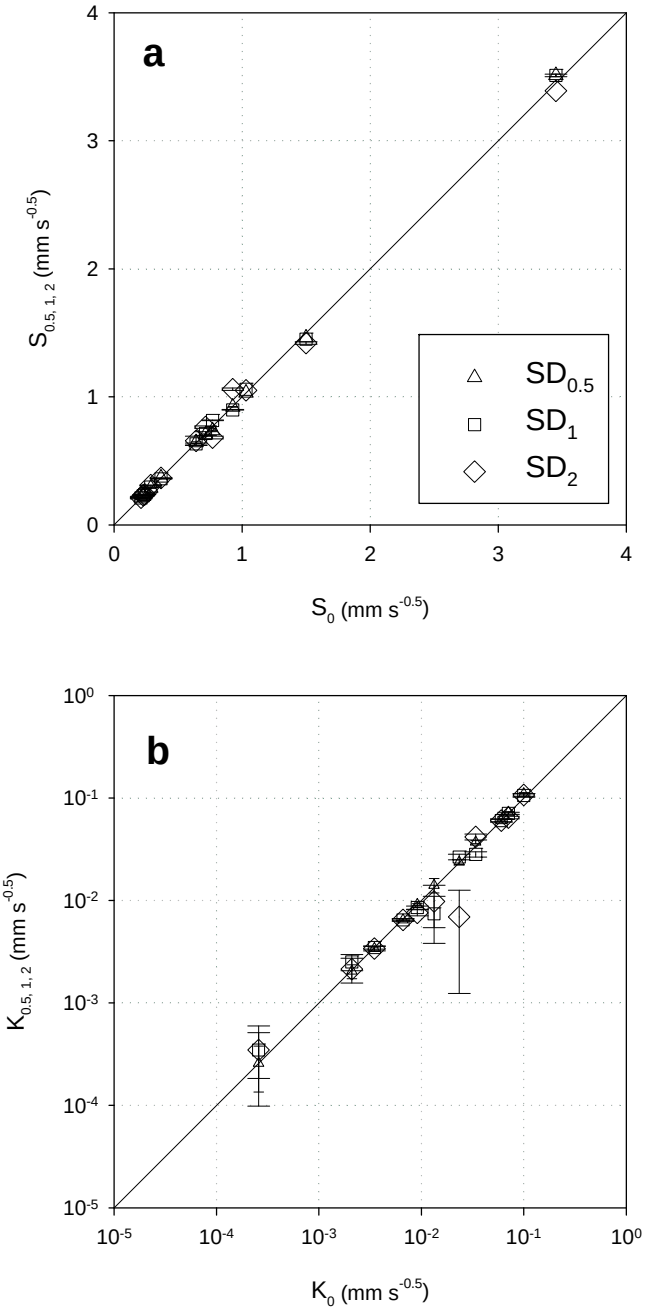

Figure 9

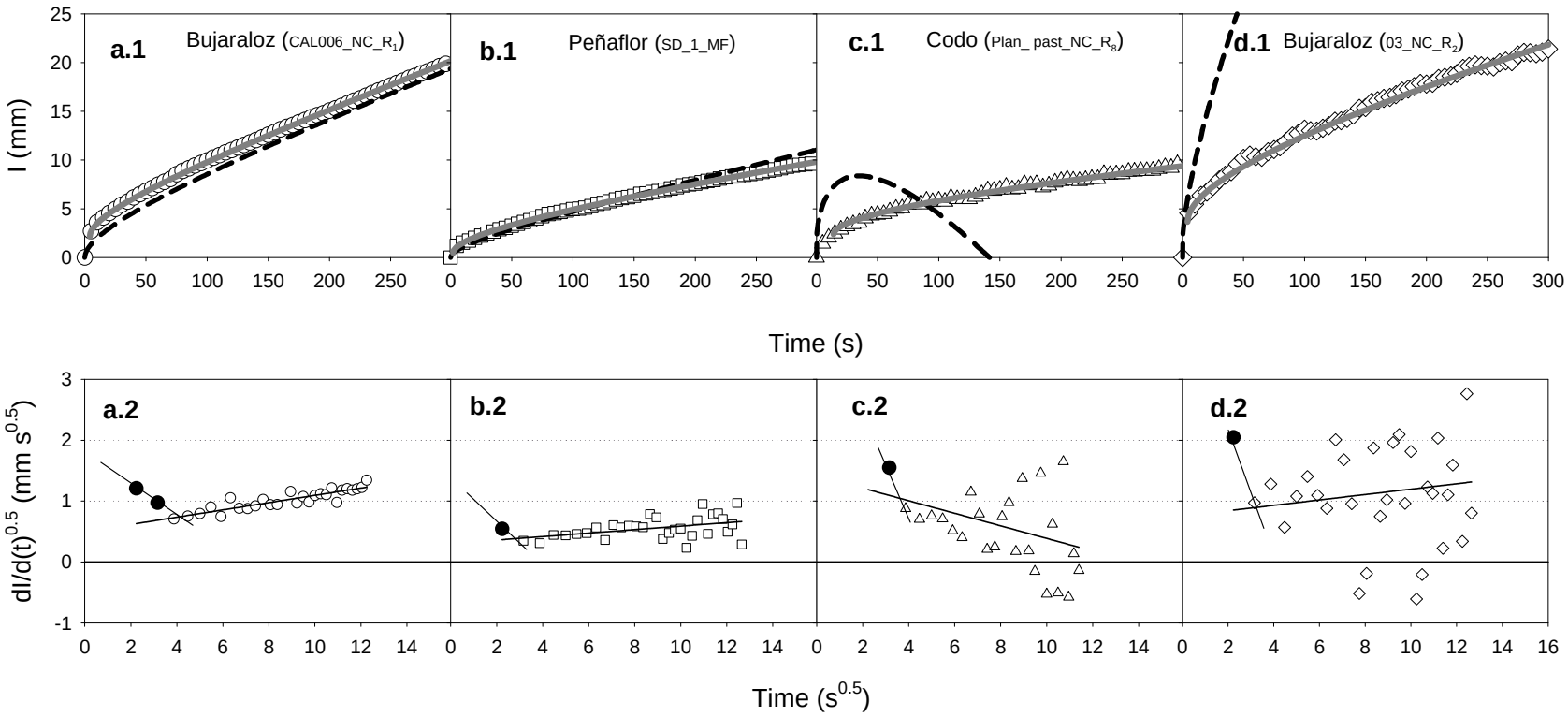
a.1
Bujaraloz (CAL006_NC_R1)
b.1
Peñaflor (SD_1_MF)
c.1
Codo (Plan_ past_NC_R8)
d.1
Bujaraloz (03_NC_R2)
I (mm)
Time (s)
a.2
b.2
c.2
d.2
dI/d(t)0.5 (mm s0.5)
Time (s0.5)

1

2 **Fig. 10.**

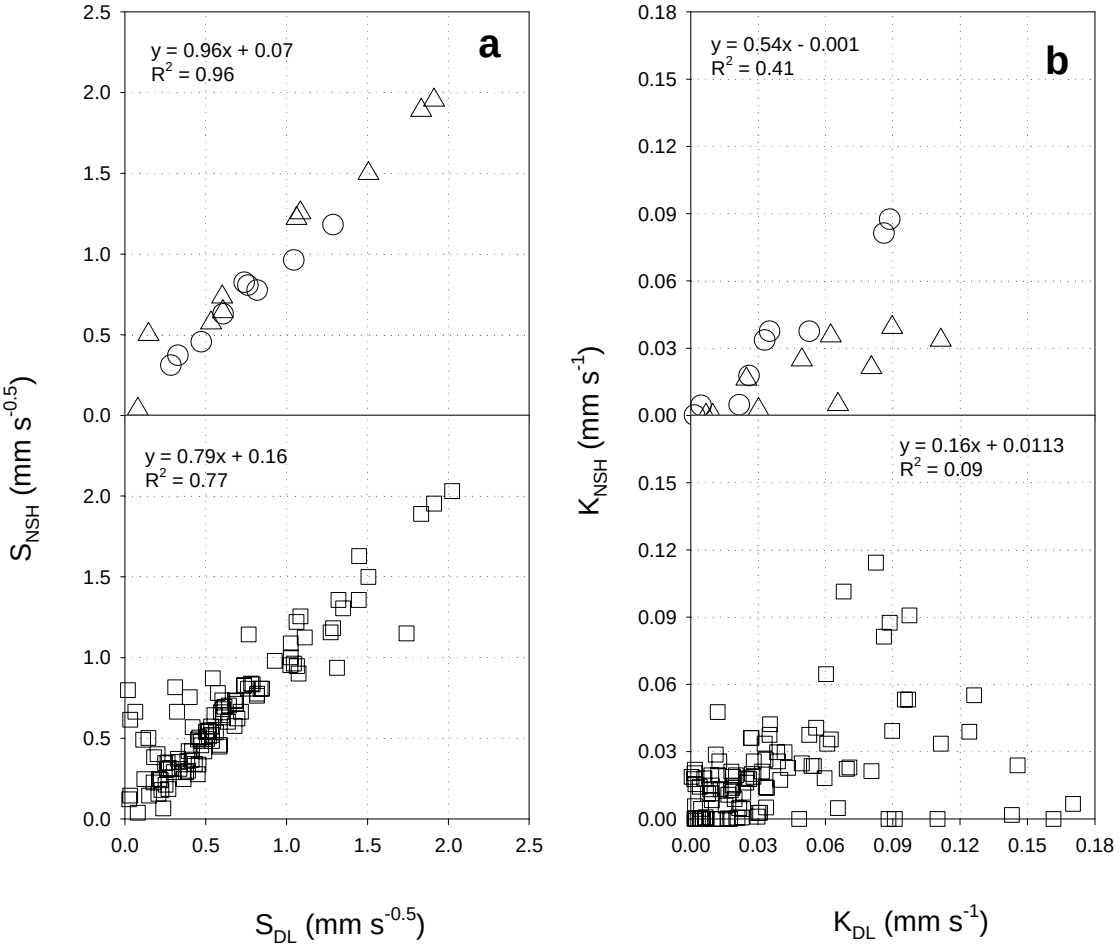
a
y = 0.96x + 0.07
R2 = 0.96
y = 0.79x + 0.16
R2 = 0.77
SNSH (mm s-0.5)
SDL (mm s-0.5)
b
y = 0.54x - 0.001
R2 = 0.41
y = 0.16x + 0.0113
R2 = 0.09
KNSH (mm s-1)
KDL (mm s-1)

Fig. 11